Journal of Power Sources 196 (2011) 10640–10651

Contents lists available at SciVerse ScienceDirect

Journal of Power Sources

journal homepage: www.elsevier.com/locate/jpowsour

A semi-empirical model considering the influence of operating parameters on performance for a direct methanol fuel cell

Q. Yang, A. Kianimanesh, T. Freiheit, S.S. Park, D. Xue*

Department of Mechanical and Manufacturing Engineering, University of Calgary, Calgary, Alberta, Canada T2N 1N4

ARTICLE INFO

Article history:
Received 24 June 2011
Received in revised form 26 August 2011
Accepted 26 August 2011
Available online 2 September 2011

Keywords:
Direct methanol fuel cell
Semi-empirical model
Operating parameters
Performance

ABSTRACT

This research focuses on modeling the relationships between operating parameters and performance measures for a single stack direct methanol fuel cell (DMFC). Four operating parameters, including temperature, methanol concentration, and methanol and air flow rates, are considered in this work. Performance of the DMFC is described by the relationship between current density and voltage. The open circuit voltage and voltage drop in the closed circuit due to resistance, activation, and concentration polarization are influenced by the operating parameters. To consider both modeling accuracy and simplicity, a semi-empirical model is developed in this work by integrating theoretical and approximation models. Experiments were designed and conducted to collect the required data and to obtain the coefficients in the semi-empirical model. The error analysis indicates that our semi-empirical model is effective for predicating the DMFC's performance. The influence of the four operating parameters on the DMFC's performance is also analyzed based on this semi-empirical model. Possible applications of the semi-empirical model in the optimal control of fuel cell systems are also discussed.

1. Introduction

Among various types of fuel cells, direct methanol fuel cells (DMFCs) have emerged in the recent years as potential power sources for portable electronic devices such as laptop computers and cell phones due to the high energy density of methanol and low power requirements of the portable electronic devices [1]. A DMFC is a kind of proton exchange membrane (PEM) fuel cell. Methanol has the advantage that it is easier to transport and refill compared with hydrogen, which is often used in other types of fuel cells. The complex steam reforming process to produce hydrogen is also eliminated in DMFC systems. In addition, since methanol is fed with a large amount of water to the anode, humidification and water management problems associated with other types of PEM fuel cells are also avoided.

To design and control DMFC systems that can be used in different applications, a good understanding and accurate modeling of DMFC behavior is necessary. From an engineering application point of view, fuel cell behavior is usually described by performance measures such as output voltage and current density, which are influenced by design and operating parameters. Typical design parameters include the type of proton exchange membrane, the catalyst and its preparation, the electrode structure, and the geometric shapes of the fuel cell components. Typical operating parameters include temperature, methanol concentration, flow rates of methanol and air, and pressures of methanol and air. In this paper, only the operating parameters are considered.

The influence of operating conditions on DMFC performance has been extensively studied through experiments [1,2]. In this research area, Song et al. [3] investigated the influence of temperature and methanol concentration on the crossover of methanol, and consequently on the open circuit voltage and cell performance. They observed that the crossover rate increases as the methanol concentration and temperature increase. They also found out that the performance improves as the temperature increases despite an increase in methanol crossover. At low methanol flow rates, the methanol concentration is too low in the catalyst layer due to mass transfer resistance resulting in low current density. When the flow rate is high enough, any further increase in the flow rate has no significant effect on the methanol concentration in the catalyst layer, thus providing no influence on cell current density. Arisetty et al. [4] studied the impact of methanol concentration on DMFC performance. Low methanol concentration reduces the reaction rate at the anode, thus resulting in a low operating voltage. However voltage does not simply increase with the increase of methanol concentration due to crossover. Yang et al. [5] studied the influence of temperature, methanol concentration, and methanol flow rate on the impedance of the fuel cell. At low temperature (e.g., 30 °C), the slow methanol oxidation reaction and oxygen reduction reaction lead to poor fuel cell performance due to high charge-transfer

* Corresponding author. Tel.: +1 403 220 4168; fax: +1 403 282 8406.
E-mail address: dxue@ucalgary.ca (D. Xue).

0378-7753/$ – see front matter © 2011 Elsevier B.V. All rights reserved.
doi:10.1016/j.jpowsour.2011.08.104

Nomenclature

A	active area (cm^2)
C_{ME}	methanol concentration (M)
E_o	open circuit voltage (V)
$E_o^{(R)}$	reversible "no-loss" cell voltage (1.21 V)
F	Faraday constant (96,485 C mol^{-1})
F_{AIR}	air flow rate (ccm)
F_{ME}	methanol flow rate (ccm)
$\Delta\overline{g_f}$	molar Gibbs energy for methanol reaction (-698.5 kJ mol^{-1})
j	current density (A cm^{-2})
j_0	exchange current density at anode (A cm^{-2})
j_{0c}	exchange current density at cathode (A cm^{-2})
k_{eff}	mass transfer coefficient at anode
k_{1O}	mass transfer coefficient at cathode
n	number of electrons transferred for each methanol molecule (6)
n_{cell}	number of cells used in a stack
N	order of reaction for methanol oxidation
N_O	order of reaction for oxygen reduction
P_{cell}	cell power density (W cm^{-2})
P_{system_con}	power consumed by supporting components of the fuel cell system (W)
P_{system_net}	net power output of the fuel cell system (W)
P_{system_total}	total power created by the fuel cell system (W)
p_O	partial pressure of oxygen (Pa)
R	gas constant (8.314472 J $(mol\,K)^{-1}$)
R_e	area-specific resistance ($\Omega\,cm^2$)
T	absolute temperature (K)
V_{cell}	cell voltage (V)
V_{stack}	stack voltage (V)
V_{system}	system voltage (V)
α_a	transfer coefficient at anode
α_c	transfer coefficient at cathode
δ	average absolute error (V)
δ_{max}	maximum absolute error (V)
η_a	anode overpotential considering activation and concentration (V)
η_{ac}	total overpotential considering activation and concentration at both anode and cathode (V)
η_c	cathode overpotential considering activation and concentration (V)
η_R	resistance overpotential (V)
σ	standard deviation (V)

resistance (CTR). At high temperature (e.g., 50 °C or 70 °C), both the enhanced kinetics and the low ohmic losses significantly improve fuel cell performance.

In recent years, many models have also been developed to describe the quantitative relationships between operating parameters and DMFC performance measures such that optimization techniques can be utilized to achieve the optimal operating conditions based on given requirements such as energy efficiency and maximum power output. In this research area, Scott et al. [6] developed a model to describe the methanol transport process that can be used to predict the effective methanol concentration at the catalyst surface and polarization at the anode. They used this model, together with an empirical model of the open circuit voltage and a cathode overpotential model, to predict the voltage and current density of the DMFC. Kulikovsky [7] introduced an analytical model for the anode side of a DMFC, taking into account the non-Tafel kinetics of electrochemical reaction of methanol oxidation, diffusion, and transport of methanol through the backing layer, and methanol crossover. Argyropoulos et al. [8] and Scott et al. [9] developed semi-empirical models considering the influence of methanol concentration and temperature on DMFC performance. Through DMFC experiments, Dohle and Wippermann [10] investigated the influence of operating conditions on the anode, the cathode, and methanol permeation to determine the parameters for a DMFC model. Ge and Liu [11] developed a three-dimensional single phase (i.e., liquid phase at anode and gas phase at cathode), multi-component mathematical model of a DMFC. The result calculated using this model was also compared with the experimental data in their research. Casalegno and Marchesi [12] investigated the influence of two-phase flow on anode performance by combining experimental and modeling approaches. Wang et al. [13] developed a semi-empirical model to derive a nonlinear equivalent circuit from a special group of impedance fuel cell models. Wang et al. [14] developed a DMFC performance model based on adaptive-network-based fuzzy inference with methanol concentration, temperature, and current as inputs and cell voltage as output. Yan and Jen [15] developed a two-phase flow model to evaluate the effect of various operating parameters such as temperature and methanol concentration on DMFC performance. Celik and Mat [16] studied the concentration of methanol through experiments and numerical methods. Zenith and Krewer [17] developed a dynamic model for a portable DMFC system.

Despite the progress in modeling DMFC behavior, these models focus on two key operating parameters: temperature and methanol concentration. Although the impact of methanol flow rate and air flow rate has been studied through experiments, a systematic approach to model the relationships between all important operating parameters and the DMFC performance measures is still required.

In our research, a semi-empirical model has been developed to describe the relationships between all major operating parameters and performance measures by integrating theoretical and approximation models for a single stack DMFC. Four operating parameters, including temperature, methanol concentration, and methanol and air flow rates, are considered in this research. Experiments have been designed and conducted to determine the coefficients for this semi-empirical model. The developed semi-empirical model has also been tested through additional experiments.

The rest of this paper is organized as follows. The existing theoretical models for DMFC's are briefly explained in Section 2. The semi-empirical model developed in this work is introduced in Section 3. Experiments and data collected for the semi-empirical model are provided in Section 4. The derived semi-empirical model and analysis considering its accuracy and the sensitivity of its coefficients are presented in Section 5. The influence of operating parameters on DMFC performance and possible applications of this semi-empirical model are discussed in Section 6. Conclusions are summarized in Section 7.

2. Direct methanol fuel cell (DMFC) and its behaviors

A direct methanol fuel cell, as shown in Fig. 1, uses methanol as fuel to generate electricity through reaction with the oxygen in the air. The overall reaction is described by [18]:

$$CH_3OH + 3/2O_2 \rightarrow 2H_2O + CO_2 \quad (1)$$

A DMFC is primarily composed of a polymer electrolyte membrane (also called proton exchange membrane, or PEM), catalyzed electrodes at the anode and cathode sides, and end plates. The polymer electrolyte membrane and catalyzed electrodes form a membrane electrode assembly (MEA). Nafion by DuPont is often used as the membrane. The electrodes, including the anode and cathode, are thick layers of carbon paper or cloth with Pt–Ru and Pt

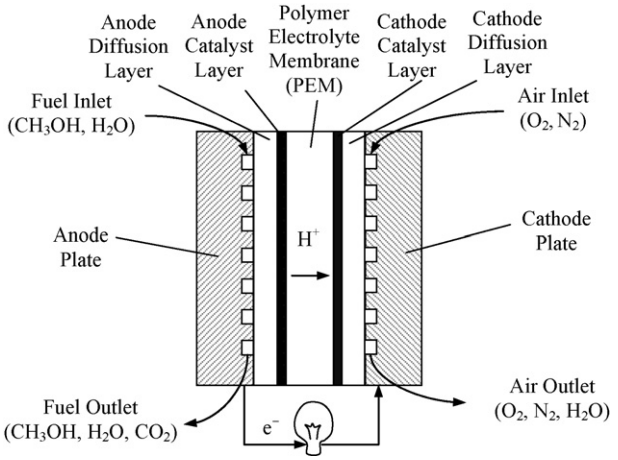

Fig. 1. Schematic diagram of a direct methanol fuel cell.

catalysts deposited on the anode and cathode, respectively. The carbon paper or cloth of the anode and cathode also diffuses methanol and oxygen to the catalysts for reaction. The graphite end plates at anode and cathode sides are used to provide methanol and air through their channels, and withdrawn current. A number of MEAs can be connected by bipolar plates, where channels are provided on both sides of each plate, to form a stack.

The reaction at the anode side is described by:

$$CH_3OH + H_2O \rightarrow 6H^+ + 6e^- + CO_2 \quad (2)$$

At the anode, the protons permeate the polymer electrolyte membrane to the cathode side, while the electrons travel through the external circuit to the cathode side to generate current. The water required comes from the methanol solution (e.g., 1 M methanol solution with 3.2% methanol and 96.8% water by mass).

The reaction in the cathode side is described by:

$$3/2O_2 + 6H^+ + 6e^- \rightarrow 3H_2O \quad (3)$$

The fuel cell performance is usually described by the relationship between current density, j ($A\,cm^{-2}$), and output cell voltage, V_{cell} (V), as shown in Fig. 2.

The power density, P_{cell} ($W\,cm^{-2}$), can be calculated by:

$$P_{cell} = V_{cell} \cdot j \quad (4)$$

The cell voltage, V_{cell}, can be calculated by [18]:

$$V_{cell} = E_o - \eta_R - \eta_{act,a} - \eta_{act,c} - \eta_{con,a} - \eta_{con,c} \quad (5)$$

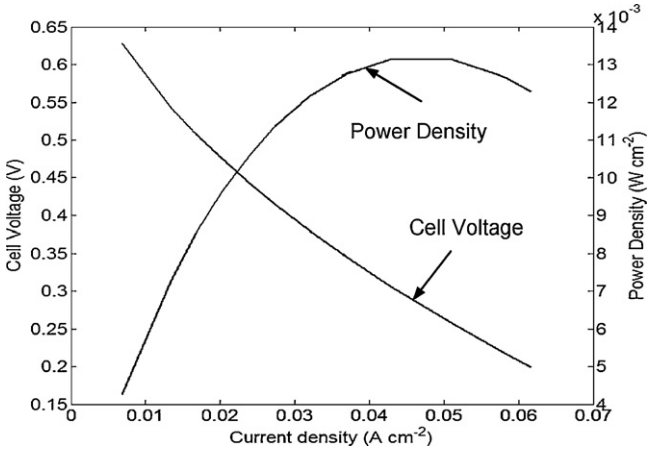

Fig. 2. Curves to model fuel cell performance.

where E_o is the open circuit voltage, η_R is the voltage loss due to ohmic polarization, $\eta_{act,a}$ and $\eta_{act,c}$ are the voltage losses at the anode and cathode due to activation polarization, and $\eta_{con,a}$ and $\eta_{con,c}$ are the voltage losses at the anode and cathode due to concentration polarization. The voltage loss is also called overpotential.

The ohmic overpotential η_R is calculated by:

$$\eta_R = R_e j \quad (6)$$

where R_e ($\Omega\,cm^2$) is the area-specific resistance of the fuel cell, particularly contributed to by the resistance of the membrane in DMFC. The area-specific resistance, R_e, is primarily influenced by the absolute temperature T (K) [9]:

$$R_e = R_0 \ \exp\left(\frac{B}{T} - \frac{B}{T_0}\right) \quad (7)$$

where T_0 and R_0 are the reference temperature and area-specific resistance, respectively, and B is a constant determined from experimental data.

According to Scott et al. [9], the open circuit voltage, E_o, can be calculated by:

$$E_o = \frac{1}{\beta_c + \beta_{ME}} \left[\beta_{ME} E^0_{ME} + \beta_c E^0_{O_2} - \ln\left(\frac{j_0 p_O^{ref}}{j_{0c}(p_O)^{N_o}}\right) - N \ \ln\frac{C_{ME}}{C_{ME}^{ref}}\right] \quad (8)$$

where E^0_{ME} and $E^0_{O_2}$ are the standard potentials at the anode and cathode when polarization is not considered, j_0 and j_{0c} are the exchange current densities at the anode and cathode, p_O^{ref} and p_o are the reference partial pressure and actual partial pressure of oxygen, N and N_o are orders of reaction for methanol oxidation and oxygen reduction defined as the powers to which the concentration terms in the rate equations are raised, and C_{ME}^{ref} and C_{ME} are the reference methanol concentration and actual methanol concentration. In Eq. (8), β_i is calculated by:

$$\beta_i = \frac{\alpha_i n_i F}{RT}, \quad (i = ME, c) \quad (9)$$

where α_i is the transfer coefficient, n_i is the stoichiometric number of electrons for a methanol molecule consumed in the reaction, F is the Faraday constant (96,485 C mol^{-1}), R is the gas constant (8.314472 J $(mol\,K)^{-1}$), and T is the absolute temperature.

Calculation of the overpotential measures considering activation and concentration polarizations at the anode and cathode is a non-trivial task. Scott et al. [9] combined the activation and concentration overpotential measures separately at the anode and cathode. In their model, the total overpotential due to activation and concentration polarizations at the anode, η_a, is calculated by:

$$\eta_a = \frac{RT}{\alpha_a F}\left[\ln\frac{jC_{ME}^{ref}}{j_0(C_{ME})^N} - N \ \ln\left(1 - \frac{j}{nFk_{eff}C_{ME}}\right)\right] \quad (10)$$

where α_a is the transfer coefficient at anode, n is the stoichiometric number of electrons for a methanol molecule consumed in the electrode reaction, and k_{eff} is the effective mass transfer coefficient, which increases with the increase in temperature and methanol concentration.

According to Scott et al. [9], the total overpotential due to activation and concentration polarizations at the cathode, η_c, is calculated by:

$$\eta_c = \frac{RT}{\alpha_c F}\left[\ln\frac{jp_O^{ref}}{j_{0c}(p_O)^{N_O}} - N_O \ \ln\left(1 - \frac{j}{nFk_{1O}p_O}\right)\right] \quad (11)$$

where α_c is the transfer coefficient at cathode, and k_{1O} is the mass transfer coefficient at cathode.

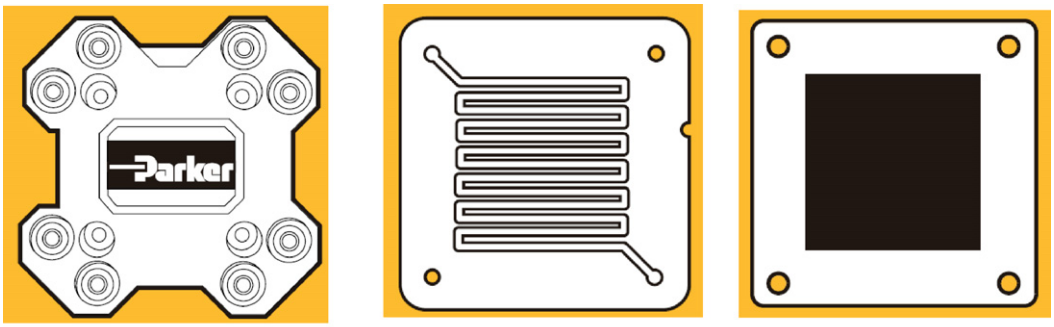

Fig. 3. Components of the TekStak™ DMFC stack [22].

Assuming the reduction of oxygen does not proceed under mass transport limitations [9], the second term in Eq. (11) is not needed to calculate the η_c. Therefore the total overpotential at anode and cathode due to activation and concentration polarizations can be calculated by:

$$\eta_a + \eta_c = \frac{RT}{\alpha_a F}\left[\ln\frac{jC_{ME}^{ref}}{j_0(C_{ME})^N} - N\ \ln\left(1 - \frac{j}{nFk_{eff}C_{ME}}\right)\right] + \frac{RT}{\alpha_c F}\ln\frac{jp_O^{ref}}{j_{0c}(p_O)^{N_O}} \quad (12)$$

Although the theoretical models are effective in describing the physical and chemical behaviors of DMFCs, these models are difficult to employ for the design and control of DMFC systems due to the complexity involved in obtaining the values of the parameters for these models. In this work, a semi-empirical model will be developed to simplify this complexity while maintaining good quality for modeling DMFC behaviors.

3. Semi-empirical model

The semi-empirical model introduced in this research was developed based on the theoretical models provided in the literature, particularly the equations given by Scott et al. [9], where the relationships between operating conditions, including temperature and methanol concentration, and DMFC performance were extensively discussed. In our semi-empirical model, the flow rates of methanol and air are also considered. Many parameters given in Scott et al. [9] were combined and simplified as coefficients in our semi-empirical model, and the values of these coefficients were obtained through an approximation process using the data collected from experiments.

In our semi-empirical model, the fuel cell voltage, V_{cell}, is described by:

$$V_{cell} = E_o - \eta_R - \eta_{ac} \quad (13)$$

where E_o is the open circuit voltage, η_R is the overpotential due to ohmic polarization, and η_{ac} is the total overpotential due to activation and concentration polarizations at both the anode and the cathode. Three sub-models, including a resistance sub-model, an open circuit sub-model and a closed circuit sub-model, have been

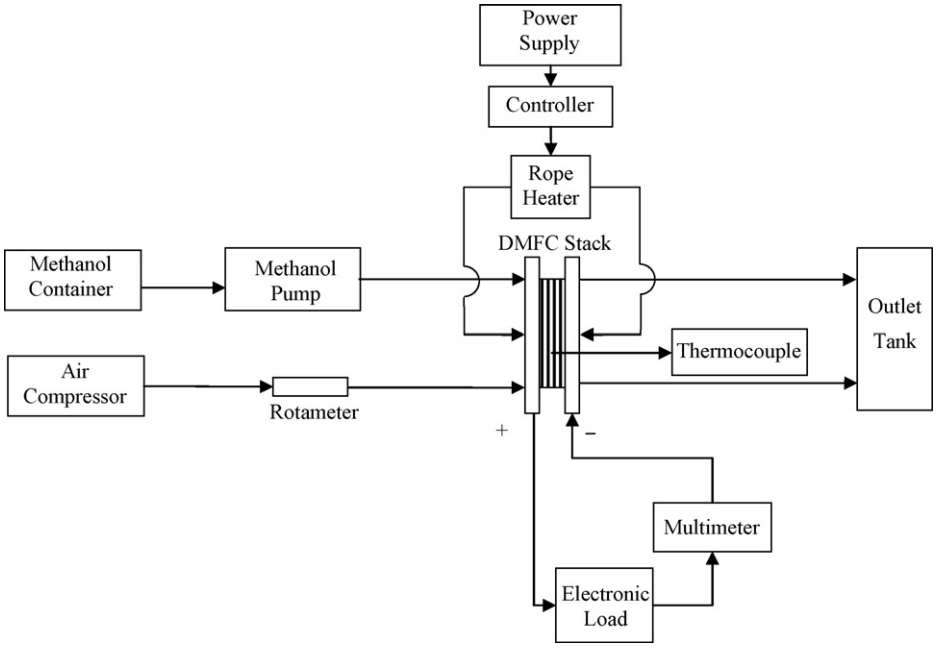

Fig. 4. Schematic diagram for the direct methanol fuel cell testing system.

developed to predict ohmic overpotential, open circuit voltage, and activation/concentration overpotential.

3.1. Resistance sub-model

The resistance sub-model aims at identifying the area-specific resistance of the DMFC, R_e, so the ohmic overpotential, η_R, can be calculated by Eq. (6).

According to Scott et al. [9], resistance of the DMFC is dominated by the resistance of the polymer electrolyte membrane. Temperature is the major factor that influences the resistance of the DMFC. Based on these observations, the area-specific resistance, R_e, in units of $\Omega\,cm^2$ in our resistance sub-model is described by:

$$R_e = a_1 e^{(a_2/T - a_3)} \tag{14}$$

where T is the absolute temperature in Kelvin, and a_1, a_2 and a_3 are experimentally determined coefficients.

3.2. Open circuit sub-model

The open circuit sub-model aims at identifying the open circuit voltage E_o in Eq. (13). From Eqs. (8) and (9) and the research result of Qi and Kaufman [19], the open circuit voltage is primarily influenced by temperature, methanol concentration, and the partial pressure of oxygen. Since the partial pressure of oxygen is coupled with the flow rate of air, in this research the open circuit voltage is modeled as a function of temperature, methanol concentration and air flow rate in the open circuit sub-model:

$$E_o = E_o^{(R)} + b_1 T + b_2 T\ \ln C_{ME} + b_3 T\ \ln(F_{AIR}) + b_4 \tag{15}$$

where $E_o^{(R)}$ is the reversible "no-loss" cell voltage, T is the temperature, C_{ME} is the molar concentration of methanol, F_{AIR} is the flow rate of air in the unit of ccm (cubic centimeters per minute), and b_1–b_4 are experimentally determined coefficients. The reversible "no-loss" cell voltage, $E_o^{(R)}$, is calculated by Larminie and Dicks [18] as:

$$E_o^{(R)} = \frac{-\Delta\overline{g_f}}{nF} = \frac{-(-698.5\times10^3)}{6\times 96,485} = 1.21\,V \tag{16}$$

where $\Delta\overline{g_f}$ is the molar Gibbs energy released from the methanol reaction ($\Delta\overline{g_f} = -698.5\times 103\,J\ mol^{-1}$), n is the number of electrons transferred for each molecule of methanol ($n = 6$), and F is the Faraday constant.

3.3. Closed circuit sub-model

The closed circuit sub-model aims at identifying the total overpotential, η_{ac}, due to activation and concentration polarizations at both the anode and cathode. According to Eq. (12), η_{ac} is influenced by temperature, methanol concentration, and flow rates of the methanol and air.

To simplify the calculation, Eq. (12) is first transformed into:

$$\eta_{ac} = \eta_a + \eta_c = \frac{RT}{\alpha_a F}\left[\ln\ j + \ln\left(\frac{C_{ME}^{ref}}{j_0}\right) - N\ \ln(C_{ME}) - N\ \ln\left(1 - \frac{1}{nFk_{eff}C_{ME}}j\right)\right] + \frac{RT}{\alpha_c F}\left[\ln j + \ln\left(\frac{p_O^{ref}}{j_{0c}}\right) - N_o\ \ln(p_o)\right] \tag{17}$$

The transfer coefficients at the anode and cathodes, α_a and α_c, are influenced by temperature, methanol concentration and current density. The partial pressure of oxygen, p_o, is coupled with the flow rate of air. In addition, the flow rate of methanol also plays a role in the activation and concentration polarizations. Based on the above considerations, the overpotential, η_{ac}, is modeled as a function of the four operating parameters by:

$$\begin{aligned}\eta_{ac} = {} & [c_1 j^3 + c_2 j^2 + c_3 j + c_4 T + c_5 C_{ME}^2 + c_6 C_{ME} + c_7] \\ & \times\left[\ln j + c_8 - c_9\left(\ln(C_{ME}) + \ln\left(1 - \frac{1}{c_{10}e^{(-c_{11}/T)}C_{ME}^2}j\right)\right)\right] \\ & +[c_{12} j^3 + c_{13} j^2 + c_{14} j + c_{15} T + c_{16} C_{ME}^2 + c_{17} C_{ME} + c_{18}] \\ & \times[\ln j + c_{19} - c_{20}\ \ln(F_{AIR})] - c_{21} j^2\ \ln(F_{ME})\end{aligned} \tag{18}$$

where j is the current density in units of $A\,cm^{-2}$, T is the absolute temperature in Kelvin, C_{ME} is the molar concentration of methanol, F_{ME} and F_{AIR} are the methanol and air flow rates in ccm (cubic centimeters per minute), and c_1–c_{21} are 21 experimentally determined coefficients.

3.4. The overall semi-empirical model

The overall semi-empirical model considering the influences of the four operating parameters on the DMFC performance is determined by combining Eqs. (6), (13)–(16) and (18):

$$\begin{aligned}V_{cell} = {} & 1.21 + b_1 T + b_2 T\ \ln C_{ME} + b_3 T\ \ln(F_{AIR}) + b_4 - a_1 e^{(a_2/T - a_3)} j \\ & -[c_1 j^3 + c_2 j^2 + c_3 j + c_4 T + c_5 C_{ME}^2 + c_6 C_{ME} + c_7] \\ & \times\left[\ln j + c_8 - c_9\left(\ln(C_{ME}) + \ln\left(1 - \frac{1}{c_{10}e^{(-c_{11}/T)}C_{ME}^2}j\right)\right)\right] \\ & -[c_{12} j^3 + c_{13} j^2 + c_{14} j + c_{15} T + c_{16} C_{ME}^2 + c_{17} C_{ME} + c_{18}] \\ & \times[\ln j + c_{19} - c_{20}\ \ln(F_{AIR})] + c_{21} j^2\ \ln(F_{ME})\end{aligned} \tag{19}$$

Values of the coefficients in the semi-empirical model for a DMFC should be obtained by collecting data of operating parameters, current density and cell voltage through experiments, and calculating these coefficient values through numerical data fitting.

4. Experiments

4.1. The direct methanol fuel cell (DMFC) – TekStak™

A DMFC kit, TekStak™, manufactured by Parker Hannifin Energy Systems was used to determine the values of the coefficients in the semi-empirical model. The DMFC stack is composed of a single cell with components of an MEA, two graphite end plates with channels for the anode and cathode, and two plastic end plates. Components of the kit are shown in Fig. 3.

The MEA is composed of a Nafion 117 membrane, an anode with catalyst of Pt–Ru, and a cathode with catalyst of Pt. The total electrode active area, A, is 10 cm^2 with a serpentine channel of 13 paths on one side of the anode or cathode as shown in Fig. 3(b). Each of the paths is 30.90 mm long, 1.27 mm wide, and 0.5 mm high. The rib between two paths is 1.07 mm in width.

4.2. Experiment setting

Fig. 4 shows the schematic diagram of the experimental set-up. Fig. 5 shows a snapshot of the experimental set-up.

The methanol is mixed with deionized water and pumped into the DMFC at a controlled flow rate using a peristaltic pump (VWR 54856-070). The air is fed into the fuel cell at a controlled flow rate using an air compressor and regulated by a rotameter (Omega FL-3861SA 150 mm). The DMFC was redesigned to replace the two plastic end plates with two aluminum end plates electrically insulated from the fuel cell with Teflon spacers such that a rope heater (Omega HTC) could be wrapped to change the working temperature of the fuel cell through a controller (Omega CSC32). The temperature inside the fuel cell is measured by a thermocouple (Omega Type K), and the temperature reading is displayed by a data acquisition unit. The anode and cathode outlet materials are collected

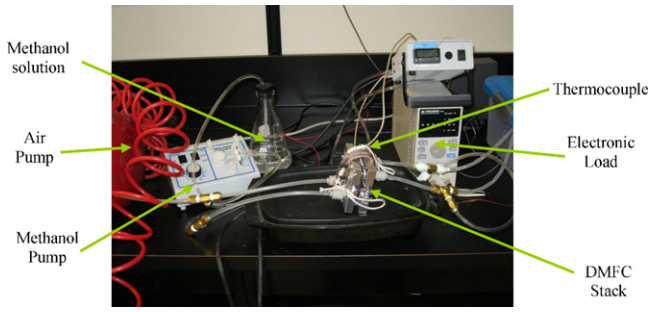

Fig. 5. A snapshot of the direct methanol fuel cell testing system.

by an outlet tank. The methanol container, the air pump, and the outlet tank are connected with the inlets and outlets of the anode and cathode of the DMFC stack using polypropylene tubes. An electronic load device (BK Precision 8540) is used to change the current density to different levels and measure the corresponding values of the voltage. In addition, a potentiostat (Gamry Reference 600) is used to measure the resistance of the fuel cell.

4.3. Design of experiments

The coefficients in the semi-empirical model were obtained by changing the operating parameters, measuring the output parameters, and calculating the values of the coefficients through a numerical data fitting technique. The operating parameters, measurement parameters, and the coefficients to be fitted are shown in Table 1.

The coefficients for the resistance and the open circuit submodels (Eqs. (14) and (15)) can be obtained directly using the operating and measurement parameters. For the closed circuit submodel, first Eq. (13) is transformed into:

$$\eta_{ac} = E_o - \eta_R - V_{cell} = E_o - R_e j - V_{cell} \quad (20)$$

to calculate the η_{ac}. In Eq. (20), the E_o is calculated using Eq. (15), R_e is calculated using Eq. (14), and V_{cell} is measured through experimentation. The coefficients of the closed circuit sub-model in Eq. (18) can then be calculated through numerical data fitting.

Four operating parameters, including temperature (T), methanol concentration (C_{ME}), flow rate of the methanol (F_{ME}), and flow rate of the air (F_{AIR}), are considered in this research. For each operating parameter, five different levels of values are selected. The values of the operating parameters, selected based on the literature review and our experimental practice, are summarized in Table 2.

For the resistance sub-model, only the temperature is selected as the operating parameter. Since five levels of this operating parameter are considered, five test cases were conducted to obtain the coefficients in the resistance sub-model at the same temperature levels shown in Table 2.

The test cases of Table 2 can be used to obtain the coefficients in both the open circuit sub-model and the closed circuit sub-model. The open circuit voltage is measured when the external resistance circuit is disconnected. Since four operating parameters and five levels are considered, the complete testing requires $5^4 = 625$ cases. To reduce the testing effort, design of experiment methodology is employed in this research to reduce the number of test cases. In this research, a uniform design (UD) methodology [20] was used to determine design points that are uniformly scattered in the design space. A uniform experimental design considering four factors at five levels gives case tables for 5, 10, 15, 20, 25, 30, 35, 40, 45, 50, and 55 tests. We selected the table with 45 cases considering fuel cell test efficiency and the quality of numerical data fitting. These 45 test cases are shown in Table 3.

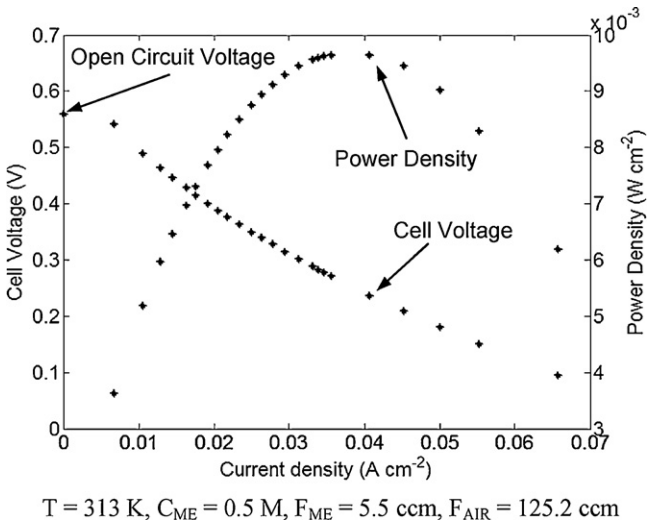

Fig. 6. Data obtained in a test case for the open and closed circuit sub-models.

4.4. Experimental data collection

The area-specific resistance measures of the fuel cell at different temperatures were obtained as shown in Table 4 using the potentiostat.

In these tests, the other operating parameters were selected as:

$C_{ME} = 0.5$ M
$F_{ME} = 3.5$ ccm
$F_{AIR} = 81.2$ ccm

Different values of these three operating parameters have also been used to test the area-specific resistance measures. It was found that the influence of methanol concentration, and flow rates of the methanol and air on the area-specific resistance was insignificant. The experimental results match with the assumptions for the semi-empirical model.

For each of the 45 test cases, the voltage at different current densities was measured as shown in Fig. 6. The voltage at $j = 0$ is the open circuit voltage E_o. By reducing the electronic load, the current density is increased and the cell voltage is decreased. For each test case, 15 or more data points were collected.

Multiple tests were conducted for some of the test cases. Three additional test cases with methanol concentration levels of 0.25 M, 0.5 M and 1 M were added because when the methanol concentration is increased, the cell voltage increases at low methanol concentration (around 0.25 M), while the cell voltage decreases at high methanol concentration (around 1 M). Other operating parameters for these three test cases were selected as $T = 323$ K, $F_{ME} = 4.5$ ccm, and $F_{AIR} = 186$ ccm. In total, 65 tests were conducted for the 48 test cases.

During the data collection process, degradation of fuel cell performance was observed for test cases repeated at different time points. In this work, a simple linear regression method was utilized to compensate the data considering this degradation. In this compensation method, a time parameter, in addition to the four operating parameters, was introduced to model the fuel cell performance. The collected data at different time points were used to obtain the coefficients in the linear regression model. The system performance measures for all test cases representing behavior at one point in time were selected to develop the semi-empirical model.

For the test cases with multiple tests, an error analysis has been conducted to study the variations of the performance measures. In

Table 1
Operating parameters, measurement parameters, and coefficients for the semi-empirical model.

Sub-model	Operating parameters	Measurement parameters	Coefficients
Resistance sub-model	T: Temperature (K)	R_e: Area-specific resistance ($\Omega\,cm^{-2}$)	$a_1, \ldots, a_3$
Open circuit sub-model	T: Temperature (K) C_{ME}: Methanol concentration (M) F_{AIR}: Flow rate of air (ccm)	E_o: Open circuit voltage (V)	$b_1, \ldots, b_4$
Closed circuit sub-model	T: Temperature (K) C_{ME}: Methanol concentration (M) F_{ME}: Flow rate of methanol (ccm) F_{AIR}: Flow rate of air (ccm)	j: Current density ($A\,cm^{-2}$) V_{cell}: Cell voltage (V)	$c_1, \ldots, c_{21}$

Table 2
Operating parameters and five levels of these operating parameters.

Operating parameter	Level				
	1	2	3	4	5
T: Temperature (K)	298	313	323	333	343
C_{ME}: Methanol concentration (M)	0.25	0.5	1	1.5	2
F_{ME}: Flow rate of methanol (ccm)	3.5	4	4.5	5	5.5
F_{AIR}: Flow rate of air (ccm)	81.2	93.6	108.7	125.2	140.8

Table 3
Forty-five test cases for the open circuit and closed circuit sub-models.

Test case no.	Levels of operating parameters				Testing case no.	Levels of operating parameters				Testing case no.	Levels of operating parameters			
	T	C_{ME}	F_{ME}	F_{AIR}		T	C_{ME}	F_{ME}	F_{AIR}		T	C_{ME}	F_{ME}	F_{AIR}
1	1	3	5	2	16	3	1	5	2	31	5	1	4	5
2	4	3	3	4	17	2	5	3	5	32	4	5	2	5
3	3	5	2	1	18	4	4	1	3	33	5	2	1	5
4	4	1	1	1	19	2	3	1	1	34	4	1	3	2
5	3	4	4	2	20	3	4	1	5	35	5	4	4	3
6	1	4	2	1	21	2	5	5	1	36	1	1	4	1
7	3	2	2	4	22	1	2	1	2	37	3	3	2	2
8	3	2	3	4	23	2	1	1	3	38	4	5	3	2
9	5	5	1	2	24	1	4	5	5	39	1	1	2	5
10	2	3	2	3	25	1	5	1	4	40	5	1	2	3
11	1	2	3	4	26	2	1	5	4	41	5	5	5	4
12	5	4	3	1	27	4	3	4	1	42	2	3	4	5
13	4	2	5	3	28	2	2	3	2	43	1	5	4	3
14	2	4	3	3	29	5	2	5	1	44	3	2	4	3
15	3	4	4	4	30	4	3	5	5	45	5	3	2	4

this work, the error bars with 95% of the confidence intervals were selected for the error analysis. The error bars for the performance measures in test case no. 2 are plotted in Fig. 7. For this test case, three tests at identical conditions were carried out to collect 68 data points at three different time points. To better show the range of error, these 68 data points were divided into 9 groups according to their current density values. The standard deviation, σ, for the data in each group was first calculated. The -1.96σ and $+1.96\sigma$ boundaries, corresponding to 95% of the confidence interval, were then used to plot the error bar for the selected data point group.

5. Results and analysis

The coefficients for the semi-empirical model were obtained based on numerical fitting of the data collected in the experiments.

Table 4
Five test cases for the resistance sub-model.

Temperature (K)	Area-specific resistance ($\Omega\,cm^2$)
298	1.42
313	1.39
323	1.11
333	1.02
343	0.98

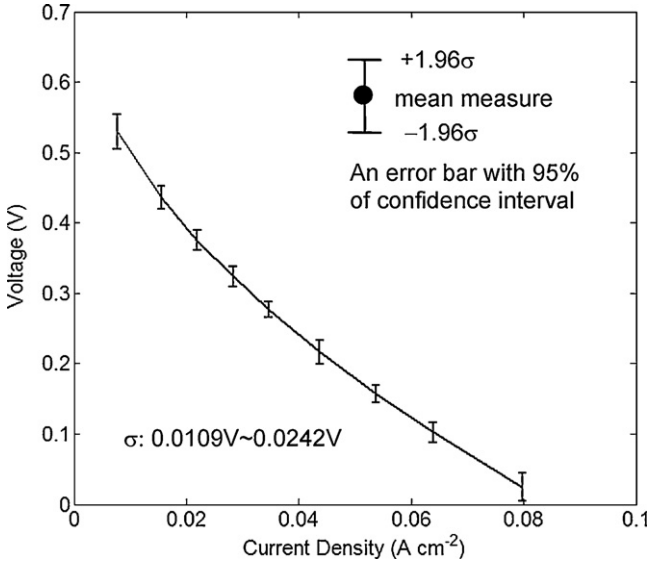

Fig. 7. Error bars for the three tests in test case no. 2.

In addition, the accuracy of the semi-empirical model and the significance of the coefficients in this semi-empirical model have also been analyzed.

5.1. Results

5.1.1. Resistance sub-model

Using the five test points given in Table 4, the coefficients in Eq. (14) were obtained through nonlinear numerical data fitting using Matlab™:

$$a_1 = 6.9897, \quad a_2 = 916.91, \quad a_3 = 4.6392$$

Substituting these coefficients into Eq. (14), we can get:

$$R_e = 6.9897e^{(916.91/T - 4.6392)} \tag{21}$$

The data and Eq. (21) are shown in Fig. 8.

5.1.2. Open circuit sub-model

For the open circuit sub-model, the data collected from the tests by changing the operating parameters of the temperature, methanol concentration, and air flow rate were used to obtain the coefficients in Eq. (15) through nonlinear data fitting with Matlab™. In this work, the data collected in the 45 test cases were used to obtain the coefficients, and the data collected in the remaining three test cases were used to evaluate the modeling accuracy. For each of the 45 test cases, the test point at $j = 0$ corresponding to the open circuit voltage was selected. When multiple tests were conducted for a test case, the average open circuit voltage was used. Therefore a total of 45 data points were used to calculate the coefficients. The coefficients obtained are:

$$b_1 = -3.7534 \times 10^{-5}, \quad b_2 = -3.1534 \times 10^{-4}$$
$$b_3 = 6.6200 \times 10^{-5}, \quad b_4 = -0.74990$$

Substituting these coefficient values and Eq. (16) into Eq. (15), an expression for the open circuit voltage is obtained:

$$E_o = 1.21 - 3.7534 \times 10^{-5}T - 3.1534 \times 10^{-4}T \ \ln C_{ME} + 6.6200 \times 10^{-5}T \ln(F_{AIR}) - 0.74990 \tag{22}$$

5.1.3. Closed circuit sub-model

For the closed circuit sub-model, first the total overpotential value, η_{ac}, for each test case was calculated using Eq. (20). In Eq. (20), E_o is calculated using Eq. (22) and R_e is calculated using Eq. (21), while V_{cell} is measured through experimentation. The calculated η_{ac}, the measured current density j, and the measured cell voltage V_{cell} at the different operating parameter test cases were used to obtain the coefficients in Eq. (18) through nonlinear numerical data fitting with Matlab™. In this work, the 62 tests including repeated test cases provided ~1200 test points used to calculate the coefficients. The coefficients obtained are:

$$c_1 = 1.2658 \times 10^5, \quad c_2 = 46196, \quad c_3 = -4281.0, \quad c_4 = -0.40290, \quad c_5 = -18.809, \quad c_6 = 18.809,$$
$$c_7 = 10.496, \quad c_8 = -3.9056, \quad c_9 = -2.9582 \times 10^{-4}, \quad c_{10} = 5.3466 \times 10^7, \quad c_{11} = 5182.4,$$
$$c_{12} = -1.2687 \times 10^5, \quad c_{13} = -46221, \quad c_{14} = 4283.6, \quad c_{15} = 0.40330, \quad c_{16} = 18.818,$$
$$c_{17} = -18.818, \quad c_{18} = -10.572, \quad c_{19} = -3.8959, \quad c_{20} = 82402, \quad c_{21} = 31.583$$

Substituting these coefficients into Eq. (18), an expression for the total overpotential is obtained:

$$\begin{aligned}\eta_{ac} = \ & [1.2658 \times 10^5 j^3 + 46196j^2 - 4281.0j - 0.40290T - 18.809C_{ME}^2 + 18.809C_{ME} + 10.496] \\ & \times \left[\ln j - 3.9056 + 2.9582 \times 10^{-4}\left(\ln(C_{ME}) + \ln\left(1 - \frac{1}{5.3466 \times 10^7 e^{(-5182.4/T)} C_{ME}^2} j\right)\right)\right] \\ & + [-1.2687 \times 10^5 j^3 - 46221j^2 + 4283.6j + 0.40330T + 18.818C_{ME}^2 - 18.818C_{ME} - 10.572] \\ & \times [\ln j - 3.8959 - 8.2402 \times 10^4 \ln(F_{AIR})] - 31.583j^2 \ln(F_{ME})\end{aligned} \tag{23}$$

5.1.4. The overall semi-empirical model

Integrating Eqs. (6), (13) and (21)–(23), the cell voltage can be calculated from the following expression:

$$\begin{aligned}V_{cell} = \ & 1.21 - 3.7534 \times 10^{-5}T - 3.1534 \times 10^{-4}T \ln C_{ME} + 6.6200 \times 10^{-5}T \ln(F_{AIR}) - 0.74990 \\ & - 6.9897e^{(916.91/T - 4.6392)} j \\ & - [1.2658 \times 10^5 j^3 + 46196j^2 - 4281.0j - 0.40290T - 18.809C_{ME}^2 + 18.809C_{ME} + 10.496] \\ & \times \left[\ln j - 3.9056 + 2.9582 \times 10^{-4}\left(\ln(C_{ME}) + \ln\left(1 - \frac{1}{5.3466 \times 10^7 e^{(-5182.4/T)} C_{ME}^2} j\right)\right)\right] \\ & - [-1.2687 \times 10^5 j^3 - 46221j^2 + 4283.6j + 0.40330T + 18.818C_{ME}^2 - 18.818C_{ME} - 10.572] \\ & \times [\ln j - 3.8959 - 8.2402 \times 10^4 \ln(F_{AIR})] + 31.583j^2 \ln(F_{ME})\end{aligned} \tag{24}$$

The effectiveness of the semi-empirical model in predicting the DMFC performance based on operating parameters will be explained in Section 5.2 through accuracy analysis. Discussion of the influence of individual coefficients on the accuracy of the semi-empirical model will be provided in Section 5.3 through sensitivity analysis.

5.2. Verification and accuracy analysis

In this research, the data from 62 tests were used as the training tests to obtain the coefficients, and the data from three tests were

Table 5
Three test cases to analyze the accuracy of the semi-empirical model.

Test case no.	T (K)	C_{ME} (M)	F_{ME} (ccm)	F_{AIR} (ccm)	n	σ (V)	δ (V)	δ_{max} (V)
1	323	0.25	4	81.2	22	0.0106	0.0082	0.0277
2	298	1	4.5	125.2	16	0.0236	0.0206	0.0312
3	343	0.5	5	140.8	15	0.0137	0.0116	0.0183
			Total		53	0.0160	0.0129	0.0312

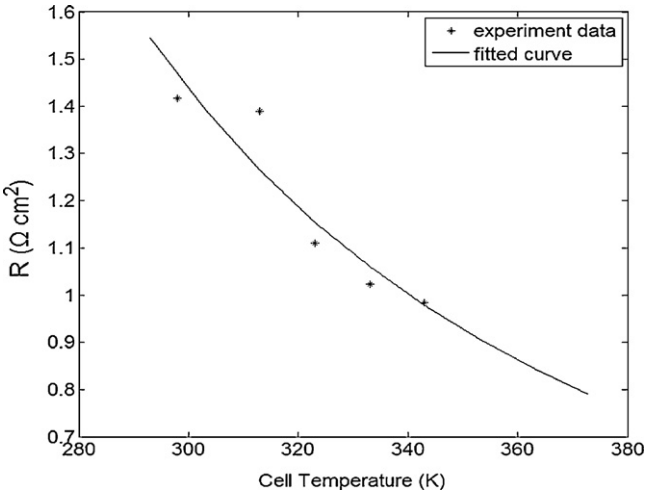

Fig. 8. Influence of temperature on area-specific resistance.

reserved to validate the semi-empirical model and test its accuracy. Fig. 9 shows the measured and predicted data for the operating conditions given in Table 5 in the three evaluation tests.

In this research, three measures, the standard deviation σ, the average absolute error δ, and the maximum absolute error δ_{max}, are used evaluate the accuracy of the semi-empirical model.

The standard deviation σ shown in Table 5 is defined by:

$$\sigma = \sqrt{\frac{\sum_{i=1}^{n}(U_i - \overline{U_i})^2}{n-1}} \tag{25}$$

where U_i is the predicted cell voltage using the semi-empirical model, $\overline{U_i}$ is the measured cell voltage from experiment, and n is the number of points in the test case.

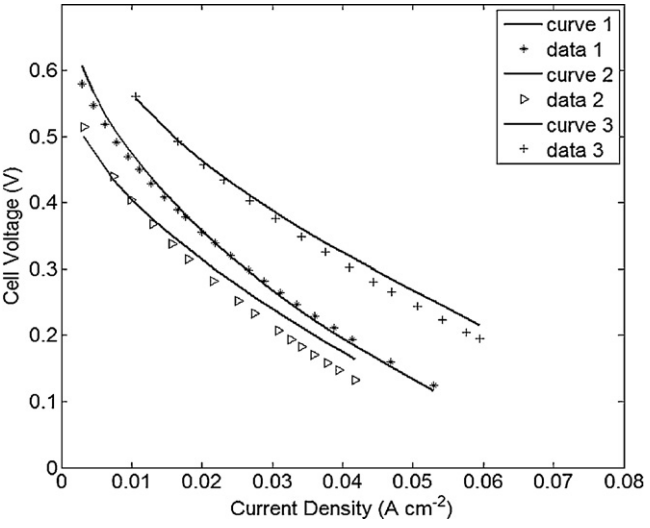

Fig. 9. Collected data through experiments and predicted curves using the semi-empirical model.

Table 6
Comparison between the errors for the evaluation tests and the training tests.

Test cases	n	σ (V)	δ (V)	δ_{max} (V)
Evaluation tests	53	0.0160	0.0129	0.0312
Training tests	1160	0.0224	0.0114	0.0568

The average absolute error δ shown in Table 5 is defined by:

$$\delta = \frac{1}{n}\sum_{i=1}^{n}\delta_i = \frac{1}{n}\sum_{i=1}^{n}|U_i - \overline{U_i}| \tag{26}$$

where the δ_i is the absolute error for the ith data point.

The maximum absolute error δ_{max} shown in Table 5 for each test case is defined by:

$$\delta_{max} = \max\{\delta_1, \delta_2, \delta_3, \ldots, \delta_n\} \tag{27}$$

The absolute error at each experimental data point between the predicted and measured voltages was analyzed to determine if there was any systematic error pattern relative to each operating parameter. Each parameter (i.e., temperature, methanol concentration, and methanol and air flow rates) was evaluated in a generalized linear model using Minitab™ against the absolute error as the outcome variable. The current density was included as a covariate. All factors were determined to be significant in contributing to the absolute error at p-values of less than 0.01. Fig. 10 shows the mean absolute error of cell voltage for each level of the experimental tests. From this analysis, it was concluded that the model error is relatively insensitive to changes in temperature and methanol concentration (average error within ~0.005 V), but has a systematic trend for the methanol and air flows, with the error trending largest at the extremes of the flow ranges. The largest absolute errors are generally found in the model to occur in general at the extreme ranges of the parameters. The largest relative errors were generally found to occur at the highest methanol concentrations.

The accuracy analysis for the 62 training tests whose data were used to obtain the coefficients of the semi-empirical model is summarized in Table 6. The errors for the training tests are

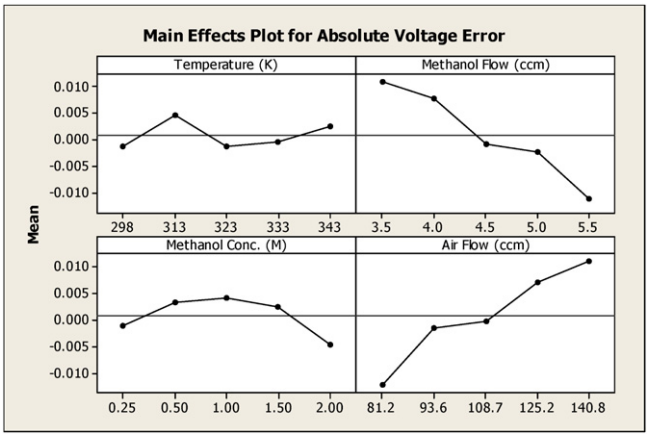

Fig. 10. Contribution of operating parameters to absolute error.

Table 7
p-Values considering the significance of the five coefficients.

Coefficient	*p*-Value
c_1	0.1084
c_3	0.6662
c_{12}	0.4931
c_{13}	0.7484
c_{18}	0.3681

Table 8
Comparison between the original and the simplified semi-empirical models.

Semi-empirical model	σ (V)	δ (V)	δ_{max} (V)
The original model with 28 coefficients	0.0160	0.0129	0.0312
The simplified model with 23 coefficients	0.0126	0.0098	0.0220

comparable with the errors for the evaluation tests. In general, the model predicted the experimental data points voltage within an accuracy of ±0.050 V approximately 90% of the time, and ±0.030 V approximately 70% of the time. On a relative basis, the model was determined to match the experimental data within a relative accuracy of ±25% approximately 90% of the time, and ±10% approximately 50% of the time. It should be noted that as a nonlinear regression model, some combinations of parameters will lead to estimation with a negative voltage, especially when these parameters are at the limits of their regression ranges. While these operating points generally would have very low voltage, nonetheless they should be treated with caution. In summary, given the experimental error, it is therefore concluded the developed semi-empirical model is effective for predicting DMFC performance based on the operating parameters.

5.3. Sensitivity analysis

The semi-empirical model has 28 coefficients in its three sub-models: three in the resistance sub-model (Eq. (14)), four in the open circuit sub-model (Eq. (15)), and 21 in the closed circuit sub-model (Eq. (18)). The scientific method requires that the model should be parsimonious, and therefore the number of coefficients should be reduced to simplify the complexity of the semi-empirical model if the quality of the model can be maintained. In this research, a sensitivity analysis considering the 21 coefficients of the closed circuit sub-model given by Eq. (18) has been conducted.

An analysis of variance (ANOVA) [21] is employed to study the contribution of each of these coefficients. First a designed experiment is used to create test cases considering the relevant coefficients. In each test case, a coefficient is increased or decreased by 5%, and the change in the performance measure is observed. Then a Matlab™ *n*-way analysis of variance (i.e., anovan) function is used to analyze the significance through the coefficient's *p*-value. A coefficient with a *p*-value less than or equal to 0.05 was considered significant, contributing to variance in the model's predicted values. If a *p*-value is larger than 0.05, the coefficient could be considered for removal from the semi-empirical model.

Among the 21 coefficients in the closed circuit sub-model given in Eq. (18), five coefficients are considered as candidates for removal due to their large *p*-values given in Table 7.

Removing these five coefficients from Eq. (18), the modified closed circuit sub-model can now be described by:

$$\begin{aligned}\eta_{ac} = {} & [c_2 j^2 + c_4 T + c_5 C_{ME}^2 + c_6 C_{ME} + c_7] \\ & \times \left[\ln j + c_8 - c_9 \left(\ln(C_{ME}) + \ln\left(1 - \frac{1}{c_{10} e^{(-c_{11}/T)} C_{ME}^2} j\right)\right)\right] \\ & + [c_{14} j + c_{15} T + c_{16} C_{ME}^2 + c_{17} C_{ME}] \\ & \times [\ln j + c_{19} - c_{20} \ln(F_{AIR})] - c_{21} j^2 \ln(F_{ME})\end{aligned} \quad (28)$$

The original semi-empirical model and the simplified semi-empirical model were evaluated using the three evaluation test cases. A comparison of the results shown in Table 8 finds that both semi-empirical models are acceptable to predict the DMFC performance based on the four operating parameters.

6. Applications of the semi-empirical model

The semi-empirical model can be used to analyze the influence of the operating parameters on the performance of the DMFC. The semi-empirical model can also be used to identify the optimal operating parameters based on the performance requirement through optimization.

6.1. The influence of operating parameters on DMFC performance

The semi-empirical model can be used to study the influence of the operating parameters on DMFC performance by changing only one of the operating parameters each time, and creating a curve of the relationship between the current density and cell voltage, as shown in Fig. 11.

The influence of the four operating parameters is summarized as follows.

- Influence of temperature (T)
  When the temperature is increased, the cell voltage will increase at different current densities as shown in Fig. 11(a). For example, consider the current density at $j = 0.045\ \mathrm{A\,cm^{-2}}$. When the temperature is increased from 298 K to 343 K, the cell voltage increases from 0.098 V to 0.179 V, a 82.6% increase in the cell voltage. Therefore high cell temperature is expected to improve the DMFC performance.
- Influence of methanol concentration (C_{ME})
  When the methanol concentration is increased, the cell voltage is increased at low methanol concentration, and cell voltage is decreased at high methanol concentration as shown in Fig. 11(b). For example, consider again the current density at $j = 0.045\ \mathrm{A\,cm^{-2}}$. When the methanol concentration is increased from 0.25 M to 0.5 M, the cell voltage increases from 0.201 V to 0.209 V, a 3.9% increase in the cell voltage. When the methanol concentration is increased from 0.5 M to 1 M, the cell voltage decreases from 0.209 V to 0.177 V, a 15.2% decrease in the cell voltage. Therefore an optimal methanol concentration is expected to improve the DMFC performance.
- Influence of methanol flow rate (F_{ME})
  When the methanol flow rate is increased, the cell voltage in general will increase, especially when the current density level is high as shown in Fig. 11(c). For example, consider again the current density at $j = 0.045\ \mathrm{A\,cm^{-2}}$. When the methanol flow rate is increased from 3.5 ccm to 5.5 ccm, the cell voltage will increase from 0.232 V to 0.260 V, a 12.5% increase in the cell voltage. Therefore high methanol flow rate is expected to improve the DMFC performance.
- Influence of air flow rate (F_{AIR})
  When the air flow rate is increased, the cell voltage in general will increase as shown in Fig. 11(d). For example, at current density $j = 0.045\ \mathrm{A\,cm^{-2}}$, when the air flow rate increases from 81.2 ccm to 140.8 ccm, the cell voltage increases from 0.113 V to 0.214 V, an 90.1% increase in the cell voltage. Therefore high air flow rate is expected to improve the DMFC performance.

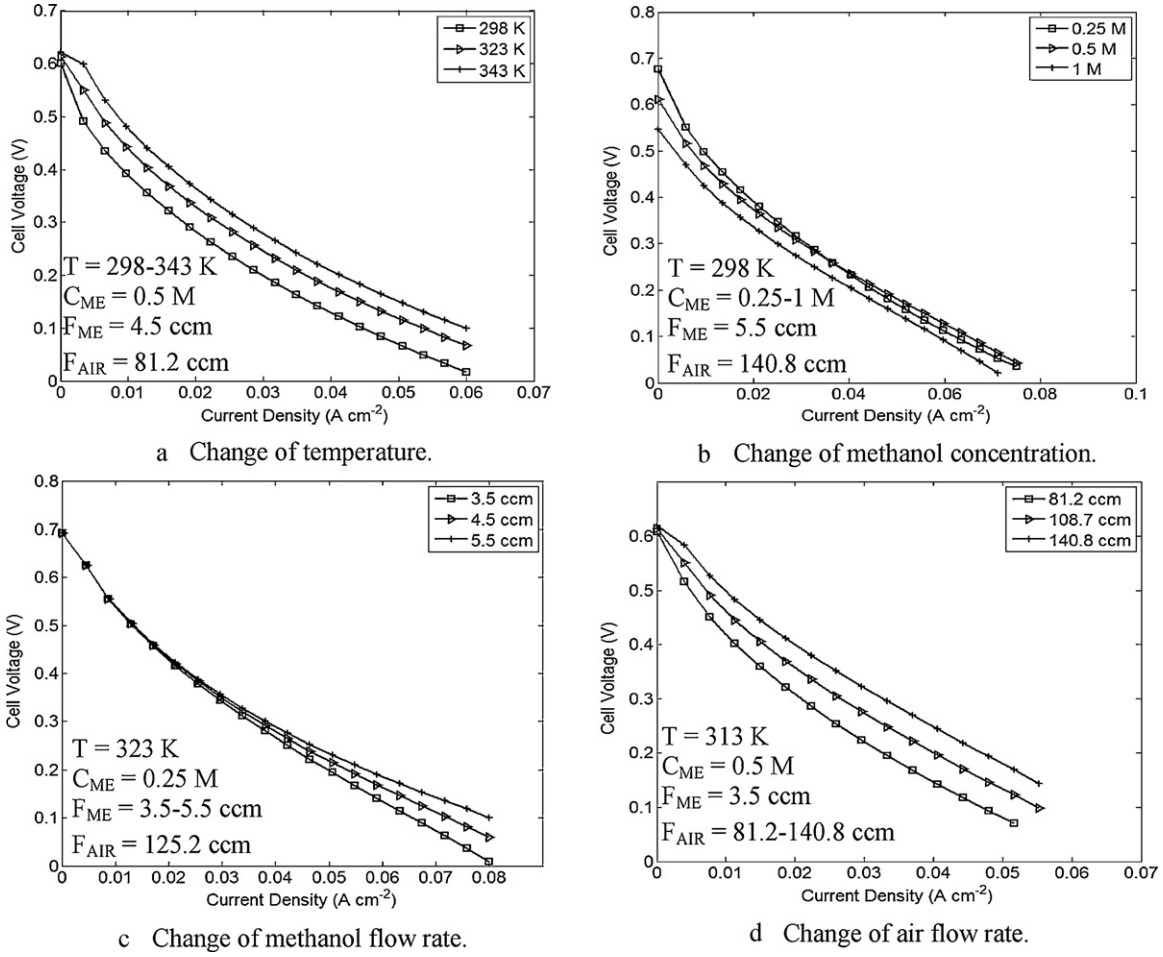

Fig. 11. Influence of the four operating parameters on DMFC performance.

6.2. Optimal control of the operating parameters

The quantitative relationships between operating parameters and fuel cell performance measures in the semi-empirical model can be used to identify the optimal operating parameters based on a given requirement.

In DMFC applications, a number of fuel cells are usually connected in series to form a stack. A number of stacks are connected to provide the required power in a DMFC system. In addition to fuel cells, other modules such as methanol container, pumps, tubes and controllers. are also needed for the fuel cell system. The operating parameters can be controlled by the controllers based on the power requirements. Therefore optimization of the operating parameters should be conducted considering the whole DMFC system.

Table 9
Different optimization models to satisfy different power requirements.

Power requirement	Optimization model
Maximum power output	$\max_{j_{max}} P_{system\_net}, j_{min} \le j \le j_{max}$
Overall power output	$\max \int_{j_{min}}^{j_{max}} P_{system\_net}\,dj$
Overall power efficiency	$\max \int_{j_{min}}^{j_{max}} \frac{P_{system\_net}}{P_{system\_total}}\,dj$

First the semi-empirical model given by Eq. (19) is used to define the cell voltage as a function of the operating parameters and the current density. Suppose this function is described as:

$$V_{cell} = f(T, C_{ME}, F_{ME}, F_{AIR}, j) \tag{29}$$

where V_{cell} is the cell voltage (V), T is the temperature (K), C_{ME} is the methanol concentration (K), F_{ME} is the methanol flow rate (ccm), F_{AIR} is the air flow rate (ccm), and j is the current density ($A\,cm^{-2}$). When n_{cell} cells are used in the stack, the stack voltage is then defined by:

$$V_{stack} = n_{cell}V_{cell} = n_{cell}f(T, C_{ME}, F_{ME}, F_{AIR}, j) \tag{30}$$

A DMFC system can be composed of a number of stacks. Suppose if m stacks are connected in series in a DMFC system, the system voltage can be described by:

$$V_{system} = mV_{stack} = mn_{cell}f(T, C_{ME}, F_{ME}, F_{AIR}, j) \tag{31}$$

The total power of the DMFC system can be obtained by:

$$P_{system\_total} = AV_{system}j = Amn_{cell}f(T, C_{ME}, F_{ME}, F_{AIR}, j)j \tag{32}$$

where A is the active area of the fuel cell. Suppose the power used by the supporting components of the DMFC system is described by

$$P_{system\_con} = g(T, C_{ME}, F_{ME}, F_{AIR}, j) \tag{33}$$

The net system power output can be calculated by:

$$\begin{aligned} P_{system\_net} &= P_{system\_total} - P_{system\_con} \\ &= Amn_{cell} f(T, C_{ME}, F_{ME}, F_{AIR}, j)j \\ &\quad - g(T, C_{ME}, F_{ME}, F_{AIR}, j) \end{aligned} \tag{34}$$

Optimization can be employed to identify the optimal operating parameters based on the power requirements. The different power requirements and optimization models that can be used to optimize the system performance are listed in Table 9.

7. Conclusions

A systematic approach to model the relationships between the operating parameters and the direct methanol fuel cell performance was introduced in this research. Four operating parameters, including temperature, methanol concentration, and flow rates of methanol and air, are considered in this work. A semi-empirical model was developed to describe the relationships. Experiments were designed and conducted to obtain the coefficients in the semi-empirical model. The accuracy of this semi-empirical model was also analyzed. In addition, the influence of the operating parameters and possible applications of the semi-empirical model were also discussed.

Characteristics of this research are summarized as follows.

1. The semi-empirical model is effective to describe the relationships between the operating parameters and the direct methanol fuel cell performance. Compared with the theoretical models that require complicated processes to obtain the physical/chemical parameters, the coefficients in our semi-empirical model can be obtained easily through numerical data fitting using data collected from experiments.
2. Through an analysis of the influence of operating parameters on the DMFC performance based on the semi-empirical model, a better understanding of the DMFC behaviors was achieved. In addition, the influence of the four operating parameters on the open circuit voltage, resistance polarization, activation polarization and concentration polarization was also achieved.
3. The modeling of the relationships between the operating parameters and the DMFC performance measures also provides a basis to identify the optimal operating parameters of the DMFC system considering different power requirements.

Our current semi-empirical model is limited to the TekStak™ DMFC. When the semi-empirical model for a different DMFC is required, new experiments need to be conducted to obtain the coefficient values of the semi-empirical model. To solve this problem, our future work will focus on development of the models considering the influence of both operating parameters and geometric parameters on DMFC performance. By adding geometric parameters to these models, the optimal design parameters, in addition to the optimal operating parameters, can also be achieved. Computational fluid dynamics (CFD) techniques will be employed in our future research.

Acknowledgements

The authors would like to thank Vien Nguyen for his early work to prepare the experiment settings. The authors are grateful for the financial support from the Canadian School of Energy and Environment (CSEE) for this work.

References

[1] R. Dillon, S. Srinivasan, A.S. Arico, V. Antonucci, Journal of Power Sources 127 (2004) 112–126.
[2] J. Ge, H. Liu, Journal of Power Sources 142 (2005) 56–59.
[3] S.Q. Song, W.J. Zhou, W.Z. Li, G. Sun, Q. Xin, S. Konton, P. Tsiakaras, Ionics 10 (2004) 458–462.
[4] S. Arisetty, C.A. Jacob, A.K. Prasad, S.G. Advani, Journal of Power Sources 187 (2009) 415–421.
[5] S.H. Yang, C.Y. Chen, W.J. Wang, Journal of Power Sources 195 (2010) 2319–2330.
[6] K. Scott, P. Argyropoulos, K. Sundmacher, Journal of Electroanalytical Chemistry 477 (1999) 97–110.
[7] A.A. Kulikovsky, Electrochemistry Communication 5 (2003) 530–538.
[8] P. Argyropoulos, K. Scott, A.K. Shukla, C. Jackson, Journal of Power Sources 123 (2003) 190–199.
[9] K. Scott, C. Jackson, P. Argyropoulos, Journal of Power Sources 161 (2006) 885–892.
[10] H. Dohle, K. Wippermann, Journal of Power Sources 135 (2004) 152–164.
[11] J. Ge, H. Liu, Journal of Power Sources 160 (2006) 413–421.
[12] A. Casalegno, R. Marchesi, Journal of Power Sources 175 (2008) 372–382.
[13] Y. Wang, G. Au, E.J. Plichta, J.P. Zheng, Journal of Power Sources 175 (2008) 851–860.
[14] R. Wang, L. Qi, X. Xie, Q. Ding, C. Li, C.M. Ma, Journal of Power Sources 185 (2008) 1201–1208.
[15] T.Z. Yan, T.C. Jen, International Journal of Heat and Mass Transfer 51 (2008) 1192–1204.
[16] S. Celik, M.D. Mat, International Journal of Hydrogen Energy 35 (2010) 2151–2159.
[17] F. Zenith, U. Krewer, Journal of Process Control 20 (2010) 630–642.
[18] J. Larminie, A. Dicks, Fuel Cell System Explained, 2nd ed., Willey, 2003.
[19] Z. Qi, A. Kaufman, Journal of Power Sources 110 (2002) 177–185.
[20] K.T. Fang, D.K.J. Lin, P. Winker, Y. Zhang, American Statistical Association and American Society for Quality 42 (2000) 237–248.
[21] D. Shasha, M. Wilson, Statistics is Easy, Morgan & Claypool Publishers, 2008.
[22] Parker, TekStak™ Educational Fuel Cell Kit – Instruction Manual and Reference Information, Parker Hannifin Energy Systems, Cleveland, Ohio, USA, 2006.